Available online at www.sciencedirect.com
ScienceDirect
Journal of Crystal Growth 305 (2007) 296–301
JOURNAL OF CRYSTAL GROWTH
www.elsevier.com/locate/jcrysgro

On the formation of well-aligned ZnO nanowall networks by catalyst-free thermal evaporation method

Zhigang Yin[a,*], Nuofu Chen[a,b], Ruixuan Dai[a], Lei Liu[a], Xingwang Zhang[a], Xiaohui Wang[a], Jinliang Wu[a], Chunlin Chai[a]

[a]*Key Laboratory of Semiconductor Materials Science, Institute of Semiconductors, Chinese Academy of Sciences, Beijing 100083, PR China*
[b]*National Microgravity Laboratory, Institute of Mechanics, Chinese Academy of Sciences, Beijing 100080, PR China*

Received 9 January 2007; received in revised form 12 March 2007; accepted 20 April 2007
Communicated by K. Nakajima
Available online 25 April 2007

Abstract

Two-dimensional ZnO nanowall networks were grown on ZnO-coated silicon by thermal evaporation at low temperature without catalysts or additives. All of the results from scanning electronic spectroscope, X-ray diffraction and Raman scattering confirmed that the ZnO nanowalls were vertically aligned and *c*-axis oriented. The room-temperature photoluminescence spectra showed a dominated UV peak at 378 nm, and a much suppressed orange emission centered at ~590 nm. This demonstrates fairly good crystal quality and optical properties of the product. A possible three-step, zinc vapor-controlled process was proposed to explain the growth of well-aligned ZnO nanowall networks. The pre-coated ZnO template layer plays a key role during the synthesis process, which guides the growth direction of the synthesized products.
© 2007 Elsevier B.V. All rights reserved.

PACS: 61.46.+w; 81.05.Dz; 81.10.Bk; 78.67.−n

Keywords: A1. Nanostructures; A3. Physical vapor deposition processes; B1. ZnO; B2. Semiconducting materials

1. Introduction

Zinc oxide (ZnO), with a bandgap of 3.35 eV and large exciton binding energy of 60 meV at room temperature, is an important optical and optoelectronic semiconductor material. ZnO one-dimensional (1-D) nanostructures, including nanowires [1], nanobelts [2], and nanotubes [3], have attracted much attention because of their remarkable physical and chemical properties. The successful synthesis of these diverse nanostructures opens numerous fields of application. Field-effect transistors (FET) [4,5], solar cells [6], and light-emitting diodes (LED) [7] based on ZnO nanowires have been realized very recently. Multidimensional ZnO nanostructures are also of great interest, and unique products such as 2-D nanosheets [8], 3-D interconnected nanowire networks [9], etc. have been synthesized recently.

Ng et al. [10] have firstly reported the preparation of a novel 2-D structure—ZnO nanowall networks (NWNs)—in which the nanowalls stand upright and are interconnected with each other. Carbothermal reduction [10–12] and MOCVD technique [13,14] are widely used to synthesize this nanostructure. The former involves the reaction of ZnO powder with carbon, in which precise control of the Au catalyst thickness and a rather high growth temperature (875–1125 °C) are needed. The latter is a more complex, costly but catalyst-free method, which usually involves the use of toxic metalorganic salts and inflammable gases. Therefore, exploring a simple, cheap, catalyst-free and low-temperature method is meaningful. In most cases for ZnO NWNs synthesis, sapphire substrates were needed because the epitaxy relation for the nanowall growth is necessary [12]. The insulating nature of sapphire might be an obstacle for the use of ZnO NWNs in electrical

*Corresponding author. Tel.: +86 1082304085; fax: +86 1082304566.
E-mail address: yzhg@semi.ac.cn (Z. Yin).

0022-0248/$ - see front matter © 2007 Elsevier B.V. All rights reserved.
doi:10.1016/j.jcrysgro.2007.04.043

devices, and thus preparation of such structure on Si is of desirable. Attempts to grow ZnO NWNs directly on silicon yielded poorly aligned products [15], or were even failed [12]. This issue may be settled by using a ZnO thin film as template layer, and such scheme has been utilized for fabricating well-aligned ZnO nanowires [16,17].

Herein, we report the synthesis of vertically aligned ZnO NWNs on ZnO-coated Si (ZnO/Si) substrate by thermal evaporation, using Zn powder and O_2 as sources. The structural and optical properties have been investigated. A possible growth route was also proposed to explain the formation of well-aligned ZnO NWNs. This structure may find use in ultra-sensitive gas sensing, photocatalysts, photoelectronics, or as templates.

2. Experimental details

ZnO NWNs were grown by thermal evaporation in a horizontal double-tube furnace. The use of a double-tube setup is to achieve a relative high vapor concentration during the growth. The zinc vapor source (0.5 g, 5 N) was loaded in a quartz boat and then inserted into the inner quartz tube (20 mm in diameter). A ZnO/Si(0 0 1) substrate was placed about 2 mm downstream of the source. The highly *c*-axis-oriented ZnO template layer (300 nm thickness) was prepared by DC magnetron sputtering at 350 °C, the details of which could be seen in Ref. [18]. Neither catalysts nor additives were used in this experiment. Before heating to the desired temperature of 530 °C, the tube furnace was evacuated to a vacuum of 1×10^{-5} mbar. Once the temperature was raised to 400 °C, oxygen was introduced into the furnace and the working pressure was kept at 0.5 mbar. No inert carrying gas was used in this study. The duration at 530 °C was 30 min. After that, the substrate was cooled down to room temperature under the forming gas. Gray-colored product was found on the substrate.

Morphology analysis was done by a high-resolution scanning electron microscope (HRSEM) Hitachi S-4800 equipped with an energy-dispersive X-ray (EDX) spectroscope. A Philips X'pert X-ray diffraction (XRD) machine was used to collect the θ–2θ scan data. To examine the crystallinity and optical properties of the as-grown ZnO NWNs, Raman scattering and room-temperature photoluminescence (PL) spectroscopy were measured with the Ar^+ (514 nm) and HeCd (325 nm) laser lines as the excitation sources, respectively.

3. Results and discussion

Fig. 1a shows the top-view SEM image of the as-grown sample. Nanowalls interconnect with each other and thus form a "foam-like" network, which assembles typical features observed in Ref. [12]. The net-like morphology can be more clearly presented by a side-view SEM image, as shown in Fig. 1a. As can be seen, the nanowalls are perpendicular to the substrate. Some tube-like products were found on the junctions of the walls, while the lengths

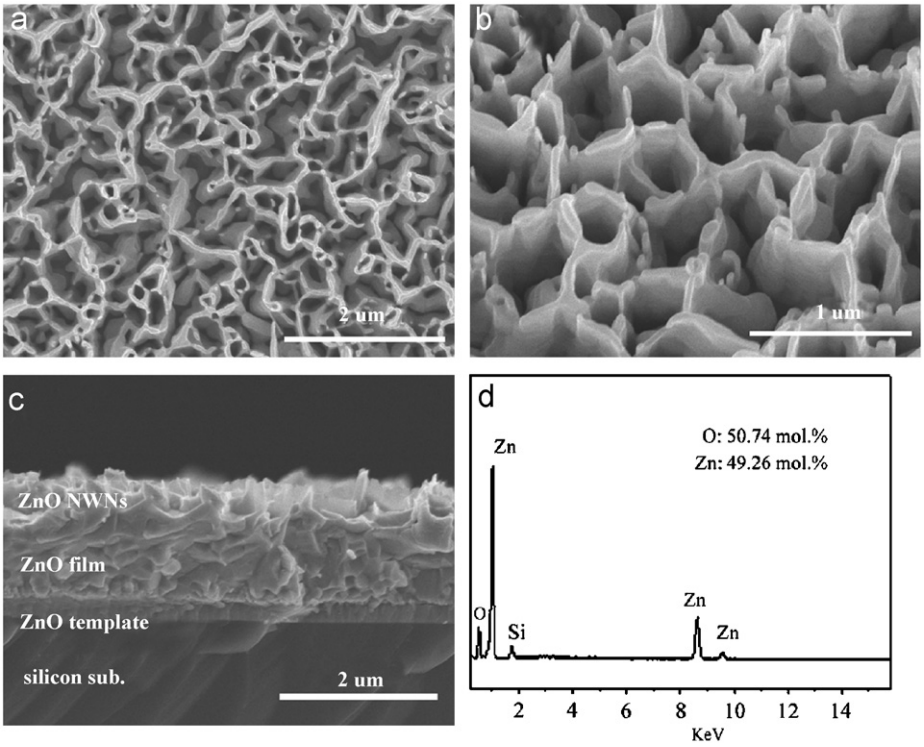

Fig. 1. SEM characterizations of ZnO nanowall networks. (a) Top-view and (b) side-view SEM images of well-aligned ZnO nanowall networks. (c) Cross-sectional SEM image; a film layer was clearly observed between the template and the nanowalls. (d) EDX spectrum of the as-received product.

of which are rather small. The nanowalls are about 50 nm thick and 500 nm high, whereon 1-D protuberances stand upright. From Fig. 1a, one can observe a typical feature of the NWNs—the roots of the walls are markedly thickened. This feature is relevant to the detailed formation mechanism of ZnO NWNs, as discussed below. The cross-sectional image is shown in Fig. 1c. The nanowalls were not directly grown on the pre-sputtered ZnO layer; instead, an additional thick layer (~1 μm) inserted between them. EDX measurement (Fig. 1d) revealed a 1:1 molar ratio of Zn to O for the product, indicating the formation of ZnO.

Fig. 2 shows the θ–2θ XRD spectra of the ZnO template film and our synthesized NWNs product. As can be seen in spectrum a, only hexagonal ZnO (0 0 2) peak appears, suggesting the fully *c*-axis preferred orientation of the film. There occurs an extra (1 0 1) peak in spectrum b, while the intensity of which is far less weak than that of the (0 0 2) peak. Also evident is the much stronger (0 0 2) peak in spectrum b. These results confirm that the as-received product is well crystallized and of highly *c*-axis oriented. The *c*-axis lattice constant of the product was calculated to be 5.206 Å, close to the bulk value [19].

Room-temperature Raman spectrum of the product was shown in Fig. 3. The spectrum was recorded within the backscattering geometry. Since the light penetration length is larger than the thickness of the as-received product, a pronounced mode E_2 (high) of the Si substrate was observed at 521 cm^{-1}. A sharp peak at 438 cm^{-1} is a typical characteristic of wurtzite ZnO and assigned to be the Raman active optical-phonon E_2 mode. A very small peak at 575 cm^{-1} was assigned as A_1 (LO) mode, and the peak at ~330 cm^{-1} might be attributed to the multi-phonon process [15,20]. The absence of the TO modes in the measurement further confirms that the ZnO NWNs are highly *c*-axis oriented, consistent with the XRD result. In the backscattering geometry, if the sample is of highly

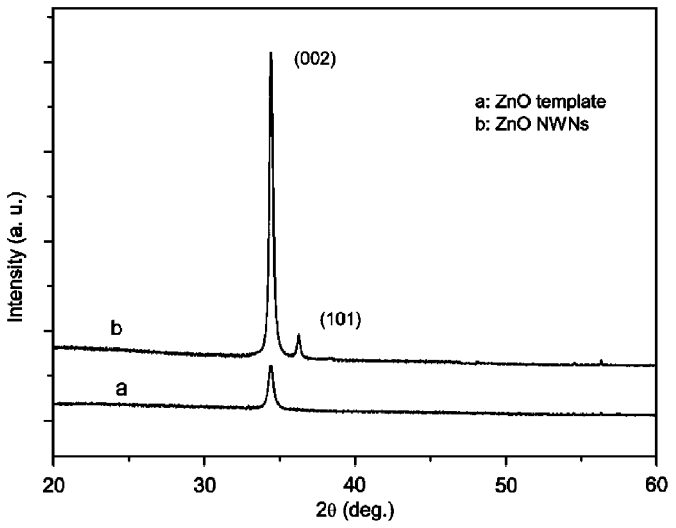

Fig. 2. XRD patterns of the ZnO template layer and the as-received product.

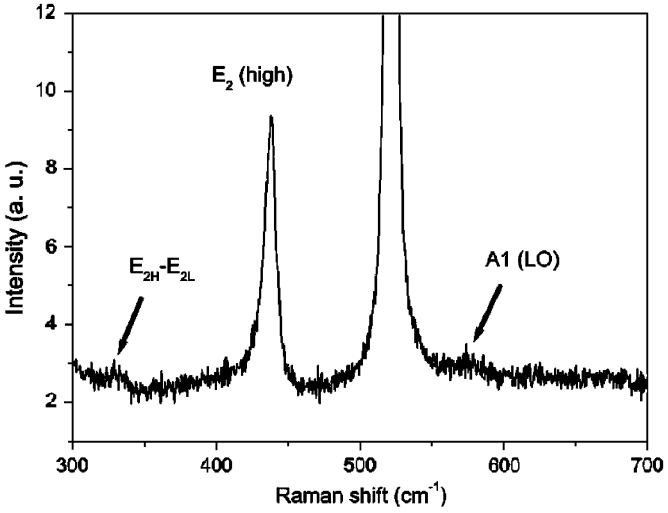

Fig. 3. Raman scattering spectrum of ZnO nanowall networks.

c-axis orientation, only E_2 and A_1 (LO) modes are allowed, while the A_1 (TO) and E_1 (TO) modes are forbidden according to the Raman selection rules [21].

We should mention that the deposition mainly occurred at the zone from ~30 mm downstream to ~15 mm upstream of the source. In this growth zone, the closer to the source, the darker the color of the deposited products. The products gathered from different places were expected to have different morphologies. To shed light on how the ZnO NWNs were initially formed, SEM images were taken of samples ~20 mm downstream of the source. Fig. 4 shows representative morphologies. In some cases, sparsely distributed ZnO nanohillocks (Fig. 4a) were clearly observed. Growth steps were found on the hillocks, which exhibit a hexagonal pattern at their initial growth stage. Under these hillocks layered a rugged polycrystalline ZnO layer. It is intriguing to mention that in certain cases, some ZnO crystallites (Fig. 4b) are hexagonal, pyramid-like in shape, assemble those reported in literature [22]. Six intersection lines of the pyramid are clearly visible. The nanohillocks tend to nucleate at the crystallite tip to reduce the local surface energy [22]. In most cases, a more complex morphology (Fig. 4c) was observed. Together with individual hillocks, hillock coalescence was found. The hillock coalescence stayed on halfway, i.e., it did not induce a 2-D film growth [23]; instead, it merely resulted in the formation of necks between the hillocks. In some places, nanowalls formed on such necks.

It should be noted that we found the Zn source surface coated with a white-colored layer once the growth was terminated and the quartz boat was took out. This means the source surface was gradually oxidized into zinc oxide during the growth. It is natural to imagine that this oxidation process reduced the Zn vapor concentration in the growth chamber. In fact, some authors [24,25] have reported the transition from film growth to nanowire growth by altering the Zn vapor supersaturation level.

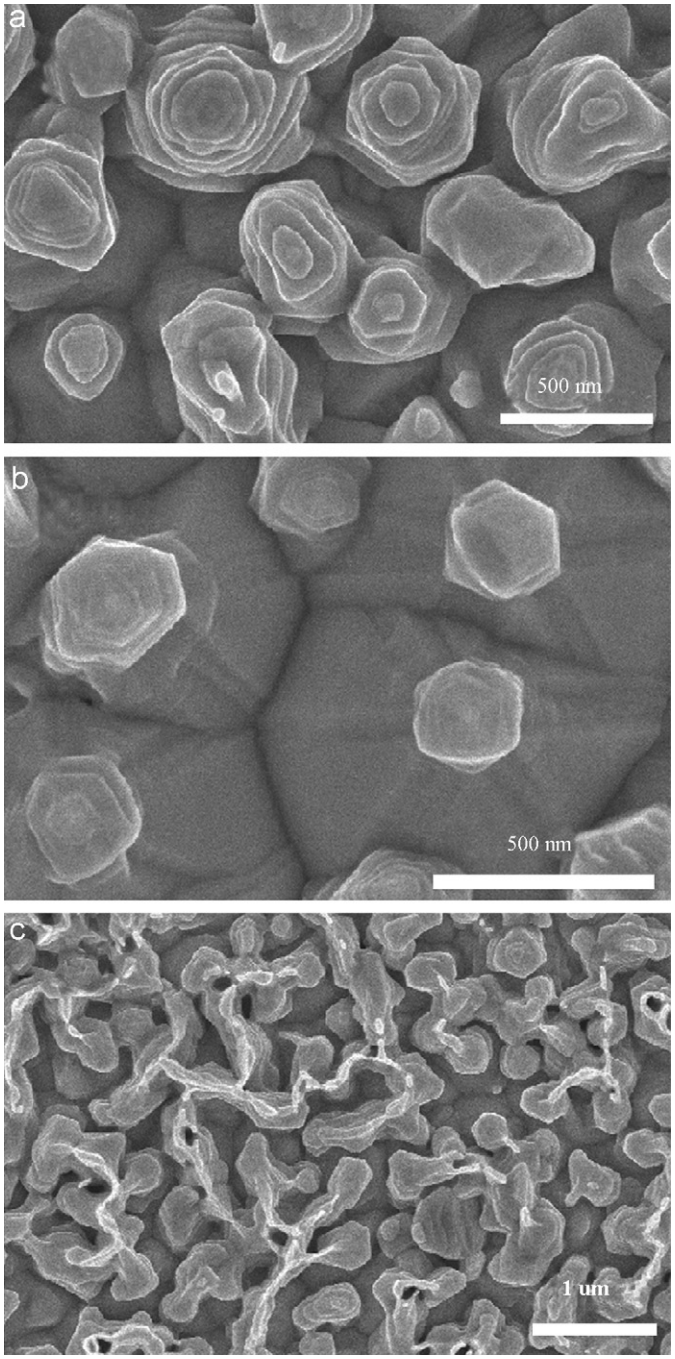

Fig. 4. SEM images of products gathered ~20 mm away from the supply boat. (a) ZnO nanohillocks formed on the polycrystalline seeding layer. (b) Pyramid-like crystallites act as the nucleation sites for the nanohillocks. (c) Nanohillock coalescence; necks between the hillocks were found, whereas in some cases nanowalls formed.

It seems highly possible that the formation of ZnO NWNs is also a Zn vapor concentration-controlled process. Different morphologies shown in Figs. 1 and 4 provide some hints for the growth route of the NWNs. In our opinion, the formation of ZnO NWNs can be divided into three stages: 2-D granular film growth, nanohillock formation and coalescence, and nanowall growth, as discussed below and illustrated in Fig. 5.

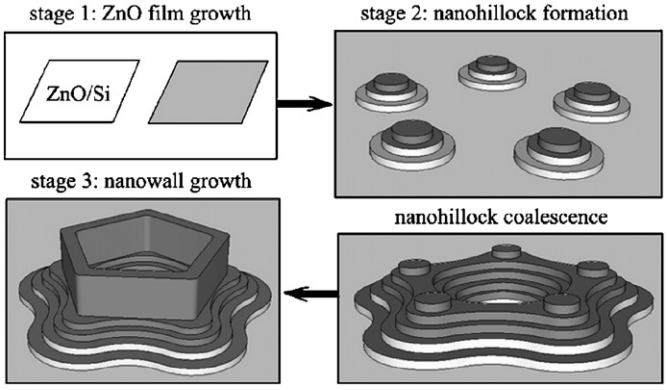

Fig. 5. Schematics of the growth route of ZnO nanowall networks.

(1) When the furnace temperature exceeded the Zn melting point (419 °C), the burst of Zn vapor provided a rather high supersaturation level for ZnO growth. High supersaturation level usually results in a lateral growth mode [24–26], and hence the formation of a thick ZnO film was favored at this stage. The pre-coated template layer provides nucleation sites and guides the growth directions of the crystallites. As a result, the synthesized ZnO film layer is of highly *c*-axis orientation.
(2) The oxidation of the Zn source gradually reduced the Zn vapor supersaturation level. When the supersaturation level was so low that the 2-D film growth became no longer favorable, the second growth stage began. A combination of 2-D lateral and 1-D vertical growth modes occurred at this stage. As a result, ZnO nanohillocks formed on the film layer. Since the ZnO seeding layer mentioned above is of *c*-axis preferred orientation, the nanohillocks tended to be vertically aligned and *c*-axis oriented. With the hillock growth and coalescence, the hillocks were prolonged in shape and necks between them appeared.
(3) Due to the continually decrease of Zn vapor concentration, further coarsening of these hillocks was not possible at a certain time, and only 1-D vertical growth was favorable [24–26]. Occurrence of 1-D protuberances in Fig. 1b is a confirmation of this estimate. The net formed by the hillocks and their necks provided special nucleation sites for the protuberances. The protuberances tended to be merged with each other to finish the local surface energy. Thus, interconnected nanowalls appeared.

Fig. 5 schematically shows the formation of a pore-like segment. The actual pores are of course not as such regular. The interconnected pore-like segments form a full network covered on the entire substrate surface. This process is quite different from the so-called VLS mechanism in the carbothermal route. Although this mechanism may qualitatively explain the general route of ZnO NWNs growth, it does not answer the details such as how to control the pore-size, the nanowall thickness and height. For better

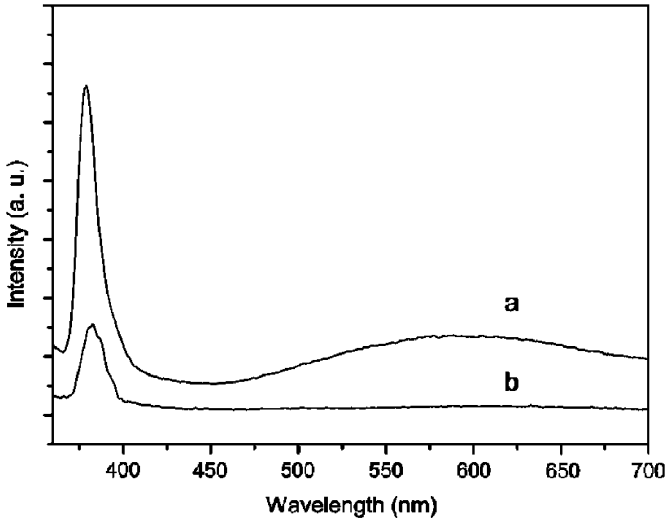

Fig. 6. Room-temperature PL spectra. Curves a and b correspond to the products shown in Figs. 1 and 4c, respectively.

understanding these issues, further studies should be done, especially in terms of temperature and forming gas dependence.

Fig. 6 shows room-temperature PL spectrum of the product shown in Fig. 1. For a comparison, PL spectrum was also measured of the product shown in Fig. 4c. The product shown in Fig. 4c exhibits much weaker UV and deep-level emissions. This result indicates a rather high luminescence efficiency of the ZnO NWNs. The ZnO NWNs exhibit a sharp UV peak at 378 nm, which is normally attributed to the recombination of free excitons. The full width at half maximum (FWHM) of this peak is 100 meV, comparable with the value reported for MBE grown films [27]. While by contrast with our result, ZnO NWNs grown by carbothermal reduction method exhibited much poorer room-temperature optical properties [11,12]. The rather high synthesis temperature, as well as the use of catalyst and additive in those studies, may account for this phenomenon. The commonly observed green emission for ZnO at around 510 nm is hardly visible; instead, there occurs a suppressed and broad orange emission centers at ~590 nm. In some papers, the orange peak was associated with excess oxygen in the lattice [28,29]. This may be relevant to the oxygen-rich growth conditions in our experiments. The sharp UV and weak deep-level emissions suggest a low defect density and fairly good crystalline quality. The excellent optical properties imply a potential use of ZnO NWNs in photoluminescent devices.

4. Conclusions

In conclusion, well-aligned ZnO networks composed of interconnected nanowalls have been synthesized on ZnO/Si substrate through thermal evaporation of metallic Zn powder at low temperature. The as-grown products exhibited fairly good crystal quality and rather low defect density. With decreasing of the Zn vapor concentration during growth, 2-D film, 1-D nanohillocks and interconnected nanowalls appeared in turn. The ZnO template layer determined the well-aligned character of the as-received products. The synthesized ZnO NWNs may be used as building blocks for photocatalysts, gas sensors, and optoelectronic devices.

Acknowledgments

This work was partly supported by the Special Funds for Major State Basic Research Projects (2002CB311905), and by the National Natural Science Foundation of China (Grant nos. 60576010, 60390072).

References

[1] M.H. Huang, S. Mao, H. Feick, H. Yan, Y. Wu, H. Kind, E. Weber, R. Russo, P.D. Yang, Science 292 (2001) 1897.
[2] P. Gao, Z.L. Wang, J. Phys. Chem. B 106 (2002) 12653.
[3] B.P. Zhang, N.T. Binh, K. Wakatsuki, Y. Segawa, Y. Yamada, N. Usami, M. Kawasaki, Appl. Phys. Lett. 84 (2004) 4098.
[4] B.Q. Sun, H. Sirringhaus, Nano Lett. 5 (2005) 2408.
[5] Z.Y. Fan, D.W. Wang, P.-C. Chang, W.-Y. Tseng, J.G. Lu, Appl. Phys. Lett. 85 (2004) 5923.
[6] M. Law, L. Greene, J.C. Johnson, R. Saykally, P.D. Yang, Nat. Mater. 4 (2005) 455.
[7] R. Könenkamp, R.C. Word, C. Schlegel, Appl. Phys. Lett. 85 (2004) 6004.
[8] S.J. Chen, Y.C. Liu, C.L. Shao, R. Mu, Y.M. Lu, J.Y. Zhang, D.Z. Shen, X.W. Fan, Adv. Mater. 17 (2005) 586.
[9] P.X. Gao, C.S. Lao, W.L. Hughes, Z.L. Wang, Chem. Phys. Lett. 408 (2005) 174.
[10] H.T. Ng, J. Li, M. Smith, P. Nguyen, A. Cassell, J. Han, M. Meyyappan, Science 300 (2003) 1249.
[11] J. Grabowska, A. Meaney, K.K. Nanda, J.-P. Mosnier, M.O. Henry, J.-R. Duclère, E. McGlynn, Phys. Rev. B 71 (2005) 115439.
[12] J.Y. Lao, J.Y. Huang, D.Z. Wang, Z.F. Ren, D. Steeves, B. Kimball, W. Porter, Appl. Phys. A: Mater. Sci. Process. 78 (2004) 539.
[13] B.P. Zhang, K. Wakatsuki, N.T. Binh, Y. Segawa, N. Usami, J. Appl. Phys. 96 (2004) 340.
[14] S.W. Kim, S. Fujita, M.S. Yi, D.H. Yoon, Appl. Phys. Lett. 88 (2006) 253114.
[15] A. Umar, Y.B. Hahn, Nanotechnology 17 (2006) 2174.
[16] L.S. Wang, X.Z. Zhang, S.Q. Zhao, G.Y. Zhou, Y.L. Zhou, J.J. Qi, Appl. Phys. Lett. 86 (2005) 024108.
[17] Y.K. Tseng, C.J. Huang, H.M. Cheng, I.N. Lin, K.S. Liu, I.C. Chen, Adv. Funct. Mater. 13 (2003) 811.
[18] Z.G. Yin, N.F. Chen, C.L. Chai, F. Yang, J. Appl. Phys. 96 (2004) 5093.
[19] A. Zeuner, H. Alves, D.M. Hofmann, B.K. Meyer, A. Hofmann, G. Kaaczmarczyk, M. Heuken, A. Krost, J. Bläsing, Phys. Status Solidi B 229 (2002) 907.
[20] H.J. Fan, R. Scholz, F.M. Kolb, M. Zacharias, U. Gosele, F. Heyroth, C. Eisenschmidt, T. Hempel, J. Christen, Appl. Phys. A 79 (2004) 1895.
[21] Ü. Özgür, Y.I. Alivov, C. Liu, A. Teke, M.A. Reshchikov, S. Doğan, V. VAvrutin, S.J. Cho, H. Morkoc, J. Appl. Phys. 98 (2005) 041301.
[22] P.X. Gao, C.S. Lao, Y. Ding, Z.L. Wang, Adv. Funct. Mater. 16 (2006) 53.
[23] Z.K. Tang, G.K.L. Wong, P. Yu, M. Kawasaki, A. Ohtomo, H. Koinuma, Y. Segawa, Appl. Phys. Lett. 72 (1998) 3270.

[24] M.C. Jeong, B.Y. Oh, W. Lee, J.M. Myoung, Appl. Phys. Lett. 86 (2005) 103105.
[25] M.C. Jeong, B.Y. Oh, W. Lee, J.M. Myoung, J. Crystal Growth 268 (2004) 149.
[26] X.D. Wang, J.H. Song, Z.L. Wang, Chem. Phys. Lett. 424 (2006) 86.
[27] Y.F. Chen, D.M. Bagnall, H.J. Koh, K.T. Park, K. Hiraga, Z.Q. Zhu, T. Yao, J. Appl. Phys. 84 (1998) 3912.
[28] S.A. Studenikin, N. Golego, M. Cocivera, J. Appl. Phys. 84 (1998) 2287.
[29] A.B. Djurišić, Y.H. Leung, K.H. Tam, L. Ding, W.K. Ge, H.Y. Chen, S. Gwo, Appl. Phys. Lett. 88 (2006) 103107.